Single Cavitation Bubble Interaction Close to Hydrophobic Surface

D. Jasikova, M. Kotek, M. Muller, V. Kopecky

***Abstract*—** The cavitation bubble has a great potential to be used for local surface hardening. Highly controlled and geometrically placed defined bubbles can easily machine the area of interest modifying the surface of material. However, the effect of pointed pressure hit can be sometimes undesirable. Usage of hydrophobic cover could shield and spread the force in certain part of working. The aim of this project was to design a setup of Laser Induced Breakup and study the effect of cavitation bubble on hydrophobic surface. The main interest was focused on the air film behavior that is created on the surface in interaction with liquids. Here we used 532nm Nd:YAG pulse laser for the cavitation bubble generation. The process and the impact of cavitation bubble was visualized using high speed shadowgraphy. We also measured the air film thickness using microPIV technique and study its behavior under increasing liquid flow impact.

***Keywords*—** Laser Induced Breakdown, Shadowgraphy, Cavitation bubble, Hydrophobic Surface, Air Film

I. Introduction

CAVITATION is mainly known for its undesirable effects in turbo machinery, marine industry; however there is a great potential for its utilization in the industry, medicine, biology, pharmacy, or tissue engineering. The presence of cavitation can cause decrease in turbo machinery efficiency due thrust lowering, increasing of drag force and appearance of additional forces on solid surfaces. Bubbles dissolved in vehicle brake system can change the density of the working liquid in an unsuitable moment and thus cause an accident. Finally, the generation of noise and vibration can also indicate the presence of cavitation. The undesirable phenomena associated with cavitation are thermal and mechanical effect during the bubble collapse. It is represented by erosion and mechanical degradation of solids. But in the first few cycles may be acoustic energy of shock waves used for surface hardening in positive way.

The process of cavitation can be generated in any kind of liquid. It is a natural process that can cause many troubles in engineering but on the other hand can be useful. These examples could be disruption of cells, bacteria or viruses, and controlled surface hardening.

The research in the field of cavitation was previously focused mainly on the investigation of bubble behavior in the vicinity of rigid or flexible boundaries; however the current investigations require including the description of response of the impacted material itself. The definition of the material response can help in development of new, more resistant structures or layers which better withstand the action of cavitation bubbles and prolong the service life of products. The key in the understanding of the cavitation interaction with various materials is the investigation of the impact of individual bubbles. The experiments focused on the investigation of the bubble wall interaction can also help to set the physical models which can be effectively used in the CFD modelling of cavitation phenomena at different scales.

Although the current state of technique is at very high level, we are still not able to produce one controllable individual bubble by pressure decrease in the liquid volume, following the cavitation definition. Substitute methods were found to generate cavitation bubble based on point source of heat [1-3]. Anyway, the generation of such bubble is not fully correct in sense of cavitation theory, the bubble behavior and process of implosion impact towards the surface is the same.

The interaction of the cavitation bubble with surfaces can be influenced by the cavitation itself as well as the surface quality. The key role plays surface roughness, initial hardness, inner stress and surface tension. In response to surface tension arose the question of interfacial behavior of cavitation if the surface is modified.

Nowadays, the main trend in surface modification is the usage of ultra-hydrophobic covers. One of the methods for the ultrahydrophobic surface covering is using nanoplasma technology [4]. The problem of hydrophobic surfaces is very complex and can be crucial to fluid mechanics, especially the problem of adhesion of liquid on a solid surface that is set as boundary condition in the most of mathematical models.

The process of ultra-hydrophobic covers could be useful in any phase of surface hardening by influencing the force impact of the bubbles, power distribution over the treated surface. As the cavitation process is stressed concentrating energy into

The results were obtained through the financial support of LO1201 under the Ministry of Education, Youth and Sports in the framework of the targeted support of the "National Programme for Sustainability I". Authors also acknowledge the support of TH01020982 project named "Efficiency improvement of energy storage and ensuring grid stability by extending the operating range of pumped storage", and the institutional support Faculty of Mechatronics, Informatics and Interdisciplinary Studies of Technical University of Liberec. This research run also with the support of Grant Agency of Czech Republic 17-19444S focused on interaction of heterogeneous liquid with flexible wall.

D. Jasikova is with the Technical University of Liberec, Department of Physical Measurement, Studentska 1402/2 Liberec 1 461 17, Czech Republic (corresponding author to provide e-mail: darina.jasikova@tul.cz).

small impacting spot, it produces high pressure peaks. In first case it can be used as a shielding of cavitating bubble impact, or following the observation as the reinforcement element of power transfer.

II. Experimental Methods

The term of cavitation originates from the Latin word *cavea* in a meaning of a hollow place. Generally, cavitation can be defined as collection of effects associated with the formation, occurrence and activity of macroscopic cavities in liquid. The cavities can be void, filled with gas, or vapor, or their mixture. Isolated cavities are often called bubbles. We distinguish several kind of cavitation by physical principle. It can be hydrodynamic, acoustic, optical, or particle cavitation.

There are also methods that enable generation of single cavitation bubble for experimental purposes. All other methods as the spark or laser generated bubbles are closer to the boiling as these are based on the evaporation of small volume of liquid. The bubbles generated by the ultrasonic field satisfy the cavitation definition, however to produce one single bubble is almost impossible.

The one of the method for bubble generation is spark in liquid, or a heated top of a wire. Once the bubble is stable, and of certain volume, it is either over heated, or expose to force impact. The convenient method for generating single cavitation bubble that can be very precisely geometrically placed in the volume of the liquid, and close to the sample, is Laser Induced Breakdown (LIB) [5-9].

The LIB method enables to generate cavitation bubble using ultrashort pulses of milijoules energies. This method is thermal breakdown based on natural plasma generation. This plasma is in form of optical breakdown, if the pulse exposure is from microseconds to femtoseconds' time. There occurs direct, multiphoton, and cascade ionization during the LIB. The significant role plays impurities of the medium, laser spot size, light wavelength, and pulse width during the breakdown. The whole mechanism of the ionization is very well explained by Kennedy [5].

A. Laser Induced Breakdown

The optical breakdown in liquid is usually produced by focusing of the laser light through suitably designed optics. The energy distribution during the growth and collapse of laser induced bubble was described e.g. by Vogel and others in [9, 10]. The authors investigated the influence of the laser pulse duration and input laser energy on the bubble dynamics and the shock waves emission.

Here we chosen green light as exciting light pulse. The absorption coefficient of 532 nm laser light is only 0.02 m^{-1} in distillated pure water. This wave length requires higher energy input to the system to induce cavitation process. For the single bubble generation we used here the setup for the LIB. The 10 ns short laser pulse was generated using Q-switched Nd: YAG New Wave Gemini pulse laser. This laser worked with one cavity for single shot generation on the wavelength 532 nm. The Q-switch signal synchronized the high speed camera running in triggering mode.

The optical setup was based on planoconvex mirror for focusing of laser light into the plasma spot instead of the plano-convex lens. The schema of this setup is seen in Fig. 1.

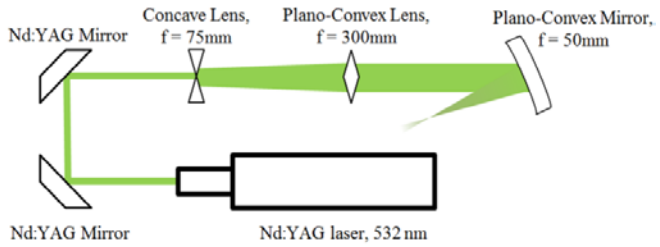

Fig. 1 Experimental setup of the reverse focusing optical setup

The energy of the laser beam was adjusted and measured with Ophir pyroelectric energy sensor. We measured the laser energy in three positions. There is seen the characteristic of laser light energy calibrated to the position of attenuator. NewWave Gemini laser enables setting of light intensity adjusting flash lamp power and fine adjustment using attenuator. The attenuator enables controllable backward loop, as an actual value is seen on the display. According to the energy calibration we did the "bubble size - laser energy" calibration to predict the final bubble sizes. There is an optical setup dependent on prediction of the bubble size – long distance microscope extension, optimal field of view and illuminating system position.

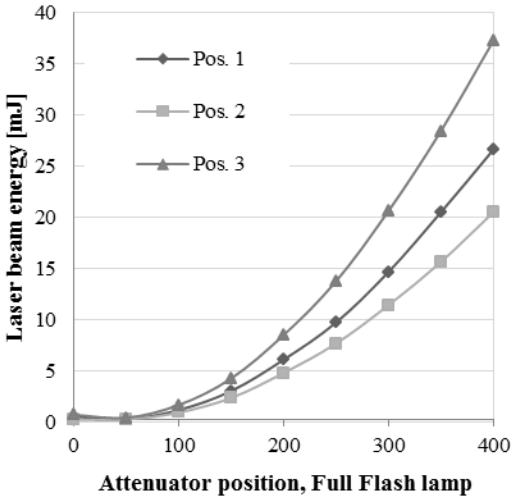

Fig. 2 The energy of laser beam measured in three positions to obtain the losses caused by optics; Position 1 was at the outcome of the laser head, position 2 was after the collimating lens, and position 3 was after the focusing mirror

The dataset of at least 20 cavitation processes for statistic evaluation was captured. This maximum bubble size was detected in each image and it was related to the energy of the laser beam. The bubble size was measured in vertical and horizontal axis and the final value represents the average value. The increase of the laser energy causes the increase of horizontal value of cavitation bubble size. This effect

corresponds with the temporal and spatial plasma evolution at the very beginning of the process.

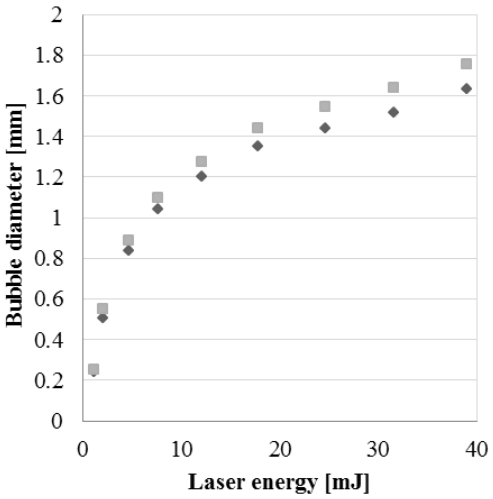

Fig. 3 Range of cavitation bubble diameter (maximal and minimal size) on the input laser energy in water on 532nm

The relation between the energy of the laser beam and the cavitation bubble size is asymptotic. This means that further increase of laser energy does not lead to significant increase of the bubble size. According to Kennedy [5], the plasma temperature shows asymptotic dependence on the laser pulse energy as well. With higher laser energy we recognized the negative influence of impurities and presence of segmentations on the bubble surface.

B. Air Film Identification

Growth of dissolved air on the hydrophobic surface can be divided into three categories: the first describe the situation, when the dissolved air is due the diffusion entrapped on the surface as the unique bubbles. These bubbles are said to be initialized in the turbulence layer in seeds. The seeds can be caused by local roughness, impurities or local change in pressure/density gradient. The growth of these single bubbles is time dependent and could grow up to 1.5 mm. Then these bubbles are changing character of the boundary layer and, of course, they actively react on local pressure changes that lead to pulsations.

The formation of the air is dependent on the contact angle of the surface – liquid interface. Here, in our study, we worked with hydrophobic surfaces, with contact angle (CA) above 90°, and with ultra – hydrophobic surfaces with CA above 120°. Increasing the contact angle leads from bubbles conglomeration to uniform air film. We were focus on the air film formation. So far, the air film was observed as the static effect, which means no liquid flow above the surface. Here we moved to examine dynamic interaction of the liquid above ultra-hydrophobic surface accompanied by formation of the air film. The dynamic interaction determines the surface endurance to cavitation bubble impact force. The parameters and the quality of the air film are dependent on the quality and uniformity of ultra-hydrophobic surface and also its roughness.

The interaction between the liquid and ultra-hydrophobic surface is followed by development of continuous layer of air film. The presence of the air film is theoretically supported by Cassie-Baxter's theory of contact angle [10]. This effect can be observed as the sample is immersed in water, and the air film is seen as a reflecting layer.

The visualization of the air film and measurement of air film thickness required to design testing samples as well as the usage of microscopy device. We suppose the air film thickness of micrometers at first. We also designed the testing sample according to knowledge of the air film formation over all hydrophobic surfaces. This means, it does not matter the geometry of the object. The testing track was designed with respect to the microscope setup as well as the surface modifying technique. We developed the testing channel with modified inner walls covered with glass to ensure the optical access. The cross-section of fabricated channel with modified wall is seen in Fig. 4.

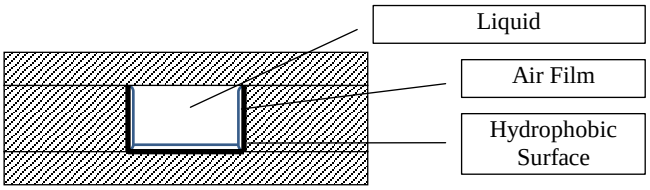

Fig. 4 Cross-section of the channel; inner walls covered with hydrophobic surface. Interaction with liquid evokes formation of the air film

Here we used microPIV technique for the visualization of the air film. The basis of microPIV technique is a laser beam, which illuminates the entire volume of the examined space. The investigated volume of liquid is enlarged with an inverted microscope, which is equipped with magnifying lens. The setup of magnifying lens and CCD camera also ensures the depth of field. The experimental setup was based on inverted microscope Leica DMIL and fitted with a set of lenses: 5x, 10x, 20x and 50x. The NewWave Gemini, Nd: YAG type pulsed laser was used for illumination of the evaluated area. The laser was of 120mJ energy per pulse in pulse length of 10ns, working on wavelength 532nm.

The images are captured with Neo CMOS chip 5,5MPixel size of 6.5 microns camera. Laser and camera system were controlled from a computer and synchronized with the external TimerBox. The depth of field depends on the distance to the measurement object from the camera lens, f-number, in the micro PIV method depth of field is dependent on the parameters of the microscope lens, index of refraction of the liquid, and the wavelength of used light. Other parameters are related to the system of lenses: NA - iris, M - total magnification microscope, and e - the distance between the pixels on the CCD camera. The depth of field is calculated using (1). The arrangement of micro PIV has a constant depth of field 4μm at 10x magnification.

$$\delta = \frac{n\lambda}{NA^2} + \frac{n.e}{NA.M} \quad (1)$$

We also used set of microscopic calibration targets for the calibration of the system to determine the magnitude coefficient. The records of calibration grid allow creating an image for further image dewarping to eliminate the image distortion due the lens system and iris.

The measurements run at 8 Hz recording frequency with 30 mW laser power at one flash. The light from the laser head was brought to investigated area with optical cable. There was captured at least 290 records for each measurement and selected Reynolds numbers.

We also used pLIF (planar Laser Induced Fluorescence) method for the air film visualization. The liquid contained high concentration (0.01g/l) of Rhodamine B to increase contrast between the liquid and air film. The dye Rh B absorbed the laser light according to Lambert-Beer law. The air film was clearly visible as the light stripe, as it is seen in Fig. 5. The visualization, when the pure water fulfilled the channel is seen in Fig. 6. The white stripe that represents the air film is still present and can be diagnosed.

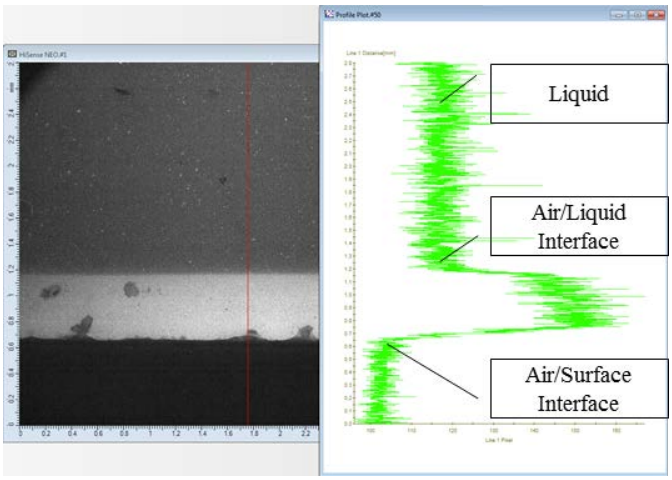

Fig. 5 Visualization of the air film close to the surface in the channel filled with Rhodamine B water solution

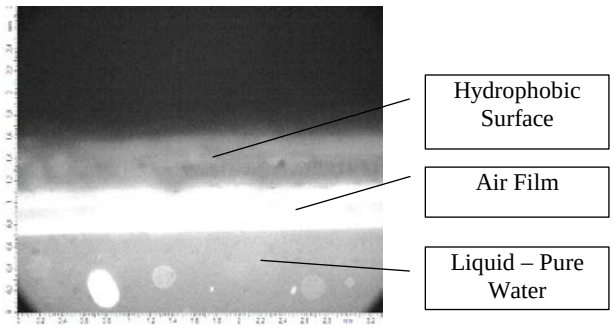

Fig. 6 Visualization of the air film close to the surface in the channel filled with pure water

We used the image processing for the detection of the air film thickness based on the pixel levels. The transition between surface and air film, as well as transition between air film and liquid is characterized with the step change. We got the dependence of the air film thickness to the liquid flow velocity, represented as Reynolds number, using this analysis [11, 12].

The outlets of test section samples were fitted with hose connection and lead to 0.5m straight hose section before the system enters the reservoir with water. The flow system is propelled by Micropump gear pump. The system was therefore enhanced with a linear precision voltage source KORADO KA3005P controllable from a PC and an adjustable voltage with an accuracy of hundredths of Volts. The flow loop is seen in Fig. 7. The range of Reynolds numbers was set from laminar to turbulent zone. This means the range between 50 to 5000 for the channel of hydraulic parameter D_h 0.08. The mean velocity was calculated from the mass flow rate that was set as accurate voltage input on the gear pump.

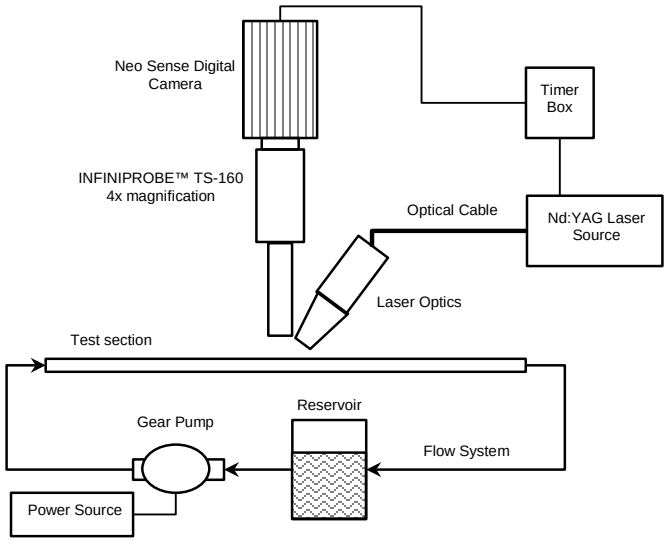

Fig. 7 Schema of experimental setup of hydraulic circuit for testing the air film thickness

C. Sample Preparation

There were prepared a set of samples for purpose of the study of cavitation bubble effect on the ultra-hydrophobic surface. The matrix material was polypropylene (PP), and glass as a reference sample. All samples were spray coated with nanopolymeric UltraEverDry®, and cold Ar+O^2 plasma treated. We treated the channel and the plain surface as the set of sample with each surface modification. The treated channel was used for air film detection and the plain surfaces were further placed in the cuvette for study of the cavitation bubble impact.

The plasma deposition includes a wide range of specific technologies, which differ from each other as technological equipment and working conditions, as well as the achieved results, i.e. the types and composition of the various deposits and their properties, structure, and chemical composition. Only some of them exhibit nanostructured character.

The one way of making nanostructured thin films of defined degrees of hydrophobicity is to use plasma jet systems. Using the plasma jet at atmospheric pressure for a modification of

macromolecular materials and surfaces is disclosed in EP 07466017.6-1226 (Klima, M. et al. 2007). The plasma jet generates plasma at atmospheric pressure and is based on principle of the hollow cathode running with high frequency (13.56 MHz).

The first set of samples was designed to cover the influence of the contact angle on the cavitation bubble behavior. There were prepared samples of PP with contact angle (CA) 110° (Sample A), CA 150° (Sample B), and CA 160° (Sample C). Sample A with hydrophobic layer obtained by direct deposition of HMDSO precursor of argon plasma generated by plasma jets. Sample B and C were prepared by the plasma, and the precursor formed HMDSO hydrophobic layers, subsequently it was applied to two different types according nanopolymers sample (to improve stability and mechanical properties). For sample B was used nanopolymers based on SiO^2 in ethanol solution (classical Nanoglass) for sample B was chosen based nanopolymers fluoro hydrocarbons in aqueous solution (rubbed into the structure ultra-hydrophobic layer). The attraction of nanopolymers can be also enforced with application of the most resistant ultrahydrophobic cover. The very mechanical resistant covers were fluoro hydrocarbons.

D. Visualization Technique

We used shadowgraphy setup for the cavitation bubble visualization. This setup consists of continuous LED matrix daylight lamp Veritas, MiniConstellation 120 – 5000 K of illuminance 92 klux in 0.5 m, equipped with optical diffuse filter. Opposite to the light source high speed CMOS camera SpeedSense was placed. This camera is working on frequency 180 kHz with spatial resolution of (128 x 128) px or lower frequency with higher resolution up to (1280 x 800) px, and the dynamic range 12 bit. The camera exposure time was to 1 µs.

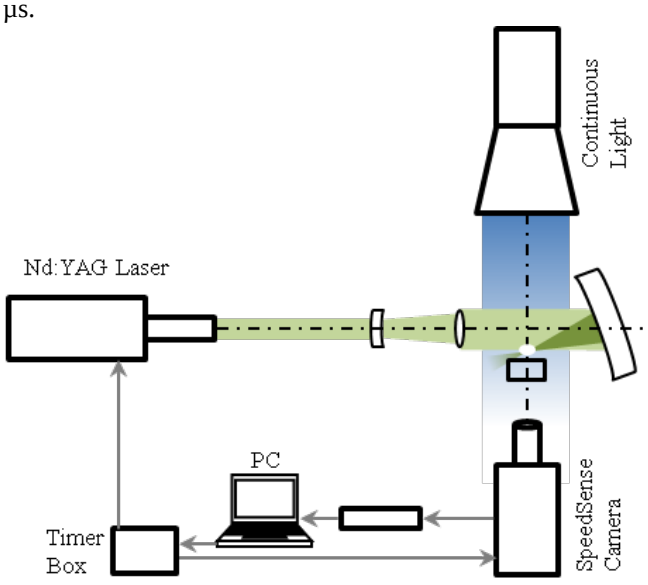

Fig. 8 The experimental setup for generation of cavitation bubble and illuminating system for high speed shadowgraph method

The camera was equipped with optical lens system INFINIPROBE™ TS-160 universal 4x macro imaging system. The lens was fitted with edge pass and long pass filter cut-on wavelength 550 nm low pass optical filter to reduce the backward laser flashes to the camera and also to eliminate the flash generated while plasmatic breakdown.

The camera was running in the triggering mode. The trigger was activated with the Q-switch pulse of laser. Once the motion was captured it dataset was moved to computer. The beginning point of the synchronization was the plasma spot accompanied by the flash. The experimental setup is seen in Fig. 8.

III. Results and Discussion

A. Air Film Thickness Estimation

Special testing samples were prepared, covered with hydrophobic surface and designed to ensure the optical access. The experimental sample setup was joined to hydraulic circuit for study of the effect of liquid flow on the behavior of the air film. The liquid flow is represented by Reynolds number. The aim of this part of research was established the critical Reynolds number under which the air film is present. The result of this study was summary graph of the static contact angle effect on quality of air film and its dependence on Reynolds number (Fig. 10). The purpose of this part of study was detecting the resistance of the air film to high Re numbers, especially in turbulent zone. The cavitation bubble implosion generates accelerated jet toward the sample surface at high velocities. Further images show the expected behavior, that air film is been thinned by cavitation bubble impact and the effect of air film is not renewable during the relaxation time between two impact hits.

Here we worked with distilled water. It is supposed that water contains certain amount of dissolved inert gases and micro-bubbles. The whole amount of present gas in water was 8 mg O_2/l at 20 °C. This value was measured with laboratory oximeter. There can be estimated total dissolved gas in the water with the knowledge of concentration of oxygen in air. The concentration of the dissolved air and amount of bubbles is strongly dependant on the partial pressure. It is said that degassed water contains about $0{,}911 \times 10^9$ nucleus of most probable size about 6 µm [14].

The formation of the air film is dependent on the flow pattern. This flow pattern is stratified into film–gas interface and could finally lead to multi-phase flow. The film structure is dependent on the geometry of the channel, roughness of the surface and it can be symmetrical or unsymmetrical.

It is said, that the air film thickness is dependant mostly on the channel geometry, that is represented by hydraulic parameter D and amount of the dissolved air α, so we can estimate the relation (2)

$$d = D\left(1 - \sqrt{1 - \alpha}/2\right) \quad (2)$$

According to previous formulation, the air film is dependent on the flow pattern, this can be expressed using Re number.

Following this formulation the interaction of the liquid flow and the air film can be divided into two regions: Re<500, and Re>500. In the first are acting macroscopic eddies instead of the second one with microscopic eddies. The interaction moved from the liquid/surface to surface/gas/liquid interface. The edge of Re 500 causes the decrease of air film thickness.

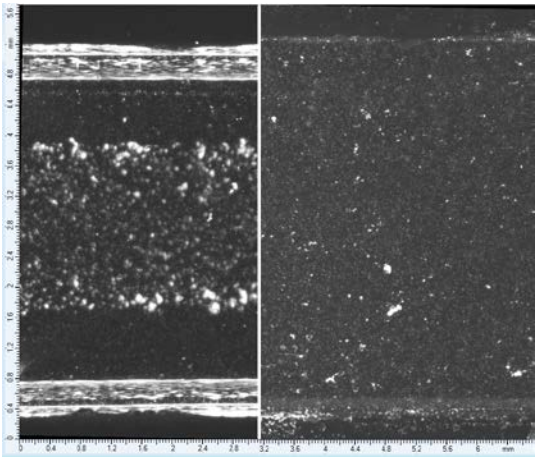

Fig 9 View into the PP channel: left side - air film upon the walls with the fluid flow Re 300, right side – the same channel with the Re 3000 - clear walls without air film.

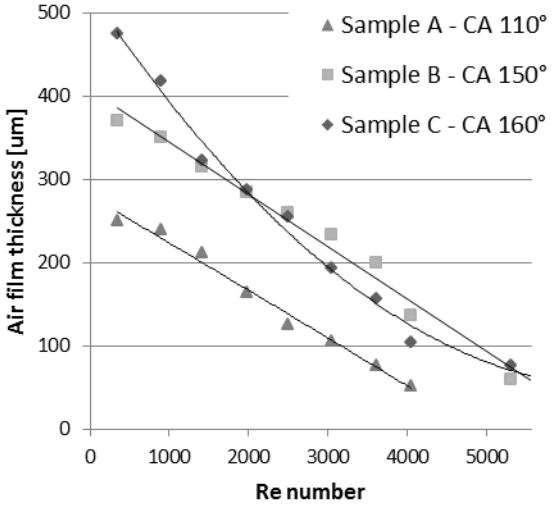

Fig. 10 Air film thickness experimentally established depending on Reynolds number

This theoretical description of the existence of the air film on hydrophobic surfaces had to be firstly proved its existence and demonstrated with the visualization technique. This would allow further description of the effect. The existence of the air film formation was proved with microscopic view. The film is formed in the region Re<500 and can be seen as light stripe that reflects the light. This stripe narrows in dependence on the Re number, respectively of the flow velocity. The visualization of the air film is seen in figure 9.

We can read from Fig. 10 that the air film thickness is strongly dependent on the initial quality that is represented with the static contact angle. The surface with the highest contact angle (160°) based on fluoro hydrocarbons nanopolymers is highly resistant to dynamic of liquid flow. The maximal Reynolds number reached with existing air film was on fluoro hydrocarbons layer, nominally Re=5600. Crossing this limit the air film is suppressed and the surface porous structure is filled with water. This process is reversible once the porous structure is completely dried.

B. Visualization of Single Cavitation Bubble

We were interested of the cavitation bubble interaction with the air film formed on the hydrophobic surface in the second part of our experimental work. The great advantage of LIB generated cavitation bubble is its space orientation to the investigated sample. The bubble can be precisely placed in the space in various distances. The most common setup is derivate from the bubble maximal size, and the major impact force is expected on 1D, or 1R of cavitation bubble. Here we present the result for 1D bubble size visualization in relation to behavior of the air film on the hydrophobic surface [13].

The maximal size of the cavitation bubble can be also precisely regulated by the input laser energy. Here we used the cavitation bubble of maximal size 1mm that corresponds to 10 mJ of input laser energy. The precisely set of optics increase repeatability of experiments and reduce losses of laser energy. The maximal size of cavitation bubble is strongly influenced by used wavelength, in our case 532nm, due the absorbance of light energy in applied liquid. The input energy also influences the lifespan of the cavitation bubbles. The bubbles generated in reverse setup have in average 40% longer exploding phase till first collapse. The energy in this setup is higher and also the focusing spot is more comprehensive and bordered. According to the energy, the bubble diameter is over 10mm at input energy 20.5mJ in one pulse of 10nm duration. The higher energy of laser light finally causes cascading energy distribution to the surroundings of the focus plasma spot. This effect leads to generation of multibubbles that are joined together and collapse irregularly.

The cavitation tests in cuvette run in 10 shots regime. The comparison of the shots and be seen in Fig. 9. The cavitation process was captured synchronously and pictures presented here are sort by the time of the cavitation process phase and for each shot. There are selected 3 fundamental changes, for the 1st, 5th and 10th laser shot and cavitation bubble impact. There are seen changes on the air film quality. There were selected a glass sample as a reference with static contact angle 60°. There is no presence of air film, or the bubbles on the surface.

The sample B with contact angle 110° formed separated bubbles on the surface. We placed the cavitation bubble above this sessile bubble to observe interaction between these two. The sessile bubble shrunk after each cavitation impact and after 10 runs it became more bordered and focused. There is seen fully developed cavitation bubble at time 38.85 μs timed from the plasma spot as the beginning of the process.

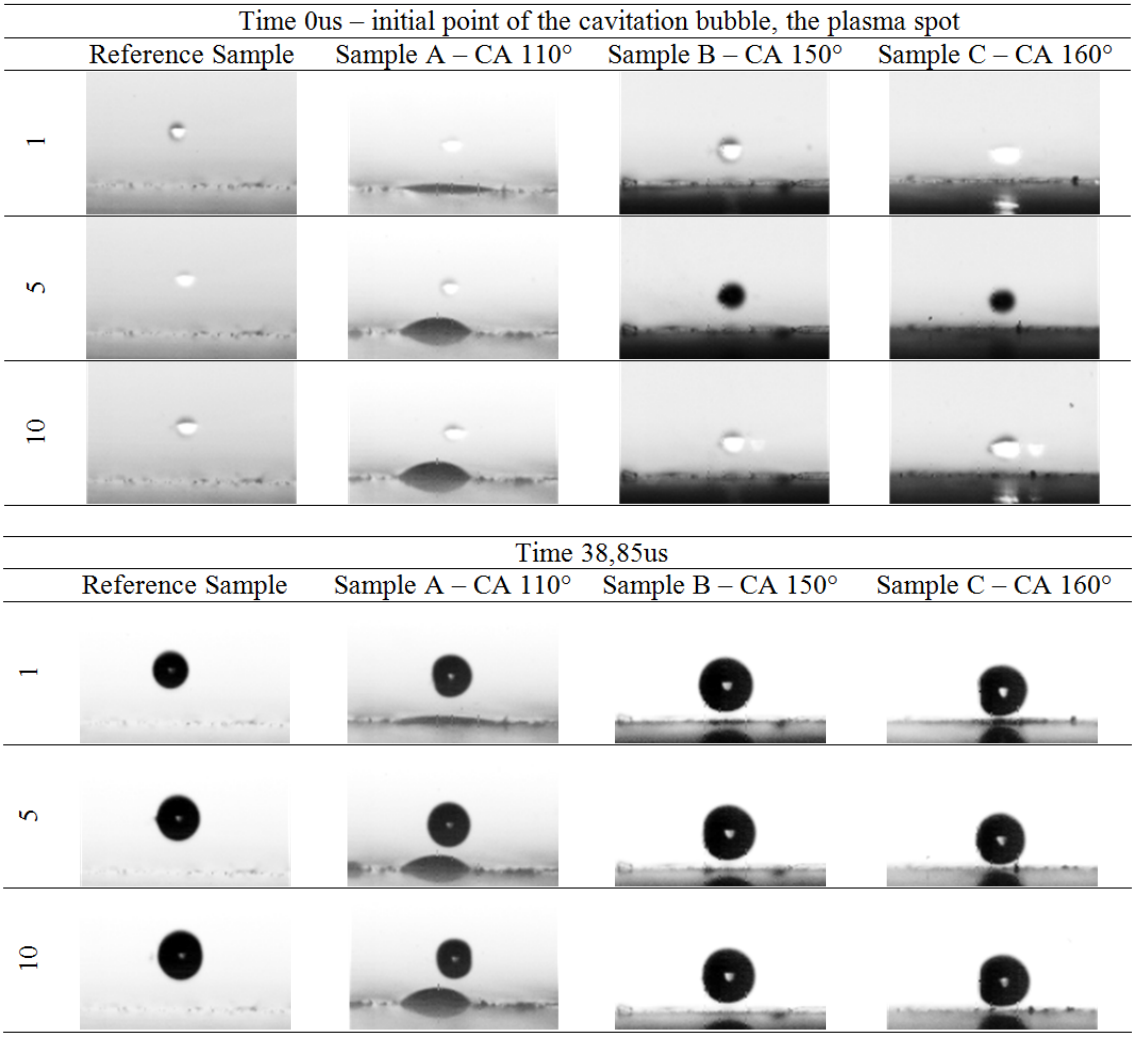

Fig. 11 The cavitation process at the initial point of plasma spot generation and fully developed cavitation bubble of maximal size at time 38.85 μs from the very start of the process

The cavitation bubble starting interaction with the air film at time 83.25 μs. There is seen the air film approach towards the cavitation bubble. This time is just before the cavitation bubble implosion. The air film is very strong affected due the reverse forces acting towards the bubble. The cavitation bubble generates the thing jet stream at the time 116.55 μs from plasma spot. There is a great pressure impact on the surface during this phase. The surface is interfered and there can be also measured great force impact. There is seen a big movement of the sessile drop as it is acted by cavitation bubble. The air film reacts in the opposite way and the pointed pressure impact is distributed over the air film surface. The background material is protected against the focused force impact, but the force is spread over the greater area. The interesting effect of the air film behaviour is sudden movement towards the cavitation bubble. This movement could be induced by the shock wave that is amplified over the volume of liquid. The air film keeps oscillating for the next at least 200 μs.

The impact of the bubble implosion is activating bordered backward wave. This surge oscillates for another 300 μs. There is seen reduce of the air film with each cavitation bubble impact. Fig. 12 shows the difference between the 1st, and 10th cavitating bubble towards the sample. The limiting number was 50 cavitation bubble of the same size impacting the surface to total retrenchment of the local air film. This impact leaves the spot 1.5x of maximal bubble size on the surface as uncovered material. Further impact of cavitation bubbles causes well-known damage of the surface structures.

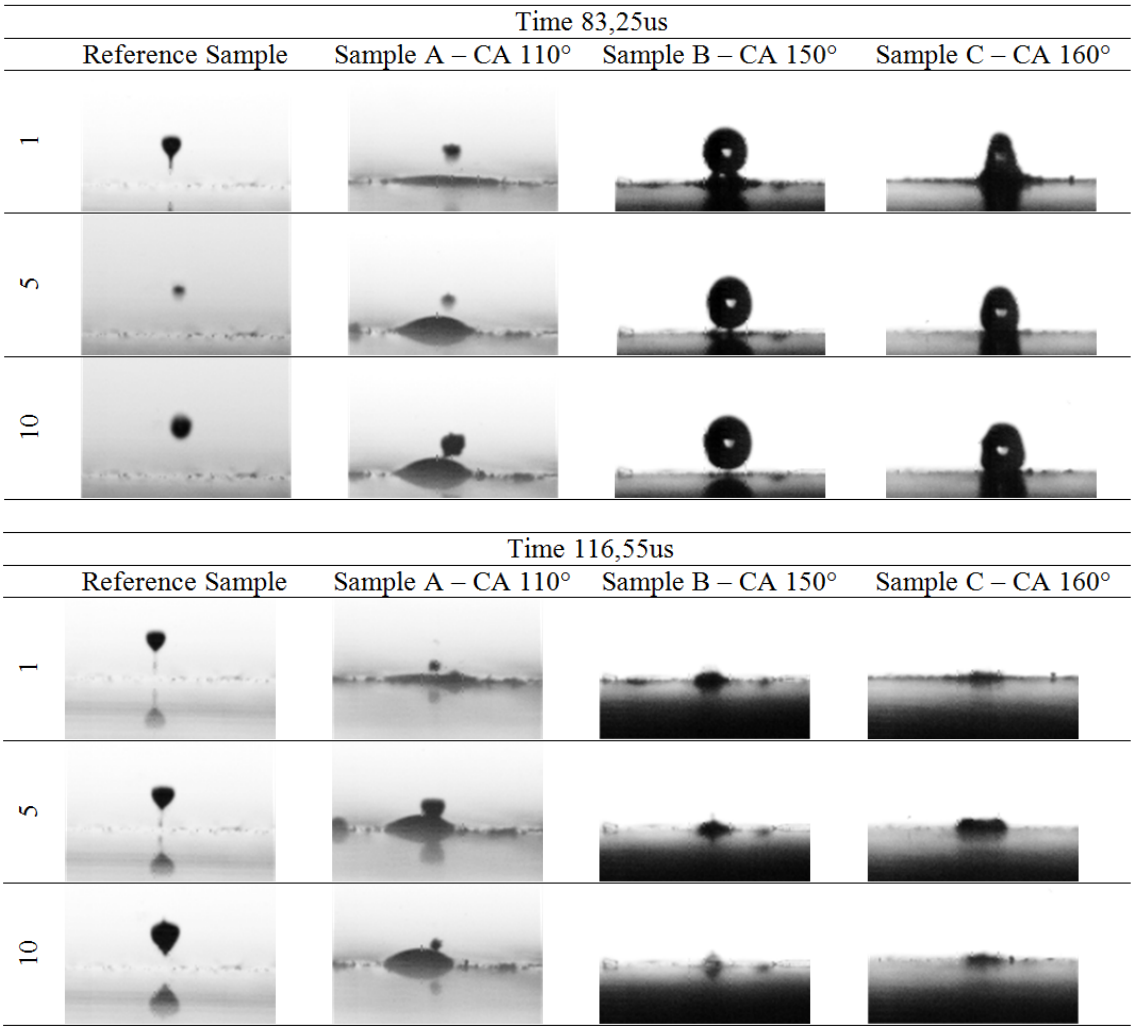

Fig. 12 Cavitation bubble impacting the solid wall at time 83.25us from beginning of the process, bubble implosion and surface interaction at time 116.55 μs from beginning of the process

IV. Conclusion

The interaction of the cavitation bubble and the air film generated on the ultra-hydrophobic surface is noticeable on the geometry 1D – the bubble is in the distance one diameter bubble maximum size far from the surface. There can be seen significant effect of the air film attraction towards the cavitation bubble during the collapse phase of the cavitation process. The following impact force is absorbed with the air film and distributed over the air film area. This effect increases the cavitation bubble impact radius up to 7D. The shockwave spreads over the air film and can be observed as oscillating pattern. The energy transmitted from the cavitation bubble to the air film is not absorbed immediately.

We also tested the repeatable generated cavitation bubbles and their effect on air film. The geometry was set as well as the distance between the bubble and surface. There was observed negative influence on the air film just after the first 5 cavitation bubbles. During the next cavitation process the air film was reduced. The effect of 10 cavitation bubbles is still reversible. There has been observed decrease of the static contact angle in the impacting area on the surfaces just after the cavitation process exposure. The surface recovered after drying.

The progressive erosion caused by cavitation bubble also further influencing the ultra-hydrophobic surface. The damaged hydrophobic treatment works no more. This regime is irreversible.

We have also tested the ultra-hydrophobic surface that creates separated bubble in the contact with fluid (Sample Glass - A). The cavitation process was set above the surface bubble and it was observed the reducing of the surface bubble till it definitively disappeared.

The great potential and proposal for the further study is a measurement of impact force over the sample. Once is proved the hardening effect in spread area this result could improve the methodic of laser ablation, or ultrasonic cavitation hardening just removing the local tension incensement that is undesirable.

The microscopic view proved the local existence of the air film, but we were interested in the situation in the whole channel geometry. For this study we used the long distance microscopy setup. We studied the complex situation of the air

film formation depending on the Re number. There could be seen the decrease of the film thickness, when Re number exceed the value for transient zone. The air film completely extinguished with high Re numbers.

Conclusiveness of this visualization was validated with the fluorescent method. The water was colored with fluorescence dye (Rhodamine B), that is concentration sensitive and the air film was visualized in the green laser light (532 nm) for the excitation. The emitted light gave us information about local concentration and the relation between water and gas.

ACKNOWLEDGMENT

Authors thank to M. Gaśic, and M. Klima fellow researchers at Masaryk University Brno for samples preparation.

REFERENCES

[1] W. Lauterborn, T. Kurz, R. Mettin, P. Koch, D. Kroninger, D. Schanz, "Acoustic cavitation and bubble dynamics, " Archives of Acoustics, 33, 2008, pp. 609-617.
[2] M. Müller, W. Garen, S. Koch, F. Marsik, W. Neu and E. Saburov, "Shock Waves and Cavitation Bubbles in Water and Isooctane generated by Nd:YAG Laser," Experimental and Theoretical Results, Proc. SPIE, 5399, 2004, pp. 275-282.
[3] D. Frost, B. Sturtevant, "Effect of Ambient Pressure on the Instability of a Liquid Boiling Explosively at the Superheat Limit, " Transactions of the ASME, 108, 1986, pp. 418-424.
[4] M. Klima, et al., "The Method of Making a Physically and Chemically Active Enviroment by Means of a Plasma jet and the Related Plasma Jet, " US 6.525.481 (2003), EP 1077021 (2005), 1998.
[5] P. K. Kennedy, D. X. Hammer, B. A. Rockwell, "Laser-induced breakdown in aqueous media, " Progress in Quantum Electronics, 21 (3), 1997, pp. 155-248.
[6] A. De-Bosset, D. Obreschkow, P. Kobel, M. Farhat, "Direct effects of gravity on cavitation bubble collapse, " Proceedings of the 58 international astronautical congress, 2007, pp. 1–5.
[7] D. Obreschkow, M. Tinguely, N. Dorsaz, P. Kobel, A. Bosset, M. Farhat, "The quest for the most spherical bubble: experimental setup and data overview, " Experiments in Fluids, 54, 2013, pp. 1503.
[8] A. Shima A., Y. Tomita, "The behavior of a spherical bubble near a solid wall in a compressible liquid, "Ingenieur-Archiv 51, 1981, pp. 243-255.
[9] A. Vogel, et al., "Energy balance of optical breakdown in water at nanosecond to femtosecond time scales, "Applied Physics B: Lasers and Optics 68, 1999, pp. 271-280.
[10] A., B., D. Cassie, S. Baxter, "Wettability of porous surfaces, "Transactions of the Faraday Society, 40, 1944, pp. 546-551.
[11] D. Jasikova, M. Kotek, S. Fialova, V. Kopecky, "A liquid interaction with ultrahydrophobic surfaces", EPJ Web of Conferences, 114, 2016, pp. 1-6.
[12] D. Jasikova, M. Kotek, V. Kopecky, "An effect of entrance length on development of velocity profile in channel of millimeter dimensions, "AIP Conf. Proc., 1745, 2016, pp. 1-6.
[13] D. Jasikova, M. Muller, M. Kotek, V. Kopecky, "The study of single cavitation bubble generated with LIB technique and its force impact on the solid wall, "International Journal of Mechanics, 9, 2015, pp. 76-82.
[14] N. I. Kolev, *Multiphase Flow Dynamics 3*, Springer-Verlag Berlin Heidelberg, 2007.